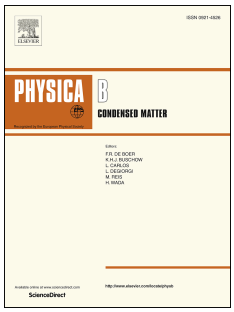

Interaction of procarbazine drug and solvent effects on pristine and embedded-zinc oxide nanotube as a drug delivery vehicle: A DFT investigation

Mohamed J. Saadh, Riyadh Abdulkareem, Omer Qutaiba B. Allela, Anjan Kumar, A.H. Shather, Devendra Pratap Rao, Lourdes Paredes Castelo, Alaa A. Omran, Ahmed Elawady

PII: S0921-4526(23)01025-6

DOI: https://doi.org/10.1016/j.physb.2023.415658

Reference: PHYSB 415658

To appear in: *Physica B: Physics of Condensed Matter*

Received Date: 31 July 2023

Revised Date: 25 December 2023

Accepted Date: 30 December 2023

Please cite this article as: M.J. Saadh, R. Abdulkareem, O.Q. B. Allela, A. Kumar, A.H. Shather, D. Pratap Rao, L.P. Castelo, A. A. Omran, A. Elawady, Interaction of procarbazine drug and solvent effects on pristine and embedded-zinc oxide nanotube as a drug delivery vehicle: A DFT investigation, *Physica B: Physics of Condensed Matter* (2024), doi: https://doi.org/10.1016/j.physb.2023.415658.

Interaction of procarbazine drug and solvent effects on pristine and embedded-zinc oxide nanotube as a drug delivery vehicle: A DFT investigation

Mohamed J. Saadh

Faculty of Pharmacy, Middle East University, Amman, 11831, Jordan

Riyadh Abdulkareem

Chemical, Biological and Radiological Safety Security Section, University of Anbar, Al-Anbar, Iraq

Omer Qutaiba B. Allela

Department of Pharmacy, Al-Noor University College, Nineveh, Iraq

Anjan Kumar*

Department of Electronics and communication Engineering, GLA University, Mathura-281406, India

A. H. Shather

Department of computer engineering technology, Al Kitab University, Altun Kopru, Kirkuk 00964, Iraq

Devendra Pratap Rao

Department of Chemistry, Coordination Chemistry Laboratory, Dayanand Anglo-Vedic (PG) College, Kanpur-208001, U.P., India

Lourdes Paredes Castelo

Chimborazo Polytechnic Higher School. Riobamba, Chimborazo 060106, Ecuador.

Alaa A. Omran

Department of engineering, AL-Nisour University College, Baghdad, Iraq

Ahmed Elawady

College of technical engineering, the Islamic University, Najaf, Iraq

***Email:** anjan1967kumar@gmail.com

Abstract

Numerous research studies have been carried out on nano-structures regarding their potential applications in drug delivery for treating cancers. Within the current work, the procarbazine (PB) drug delivery ability of a pure ZnO nanotube (PZnO-NT) and X-doped (X= Al, Ge, and In) ZnO-NT is inspected through DFT computations. The results demonstrates that PZnO-NT isn't suitable for the PB drug delivery. We showed that doping the Al, Ge, and In atoms into the ZnO-NT structure changes the adsorption energy (AdE) of PB from -6.9 to -26.4, -28.7, and -31.5 kcal/mol, respectively. Moreover, there is a substantial amount of charge transfer from PB to the doped ZnO-NT based on the natural bond orbital analysis. Using water solvent changes the AdE of the drug on the In-doped ZnO-NT from -31.5 to -29.8 kcal/mol. Hence, based on the computations undertaken within this work, the X-doped ZnO-NT can be utilized as a suitable PB carrier.

Keywords: ZnO nanotube, Procarbazine drug, Drug delivery, DFT

1. Introduction

One of the commonly used anti-cancer medications for the treatment of cancer is procarbazine (PB). Moreover, it is one of the cytotoxic chemotherapeutic drugs used for the treatment of Hodgkin's lymphoma and most brain-related cancers [1]. Being on the WHO list of essential medicines, PB was verified in 1969 for the first time [2-6]. PB is usually taken by mouth. Low blood cell counts, nausea, fatigue, and depression are the common side effects associated with PB [7, 8]. It is possible to use drug delivery systems (DDSs) in order to overcome such drawbacks [9]. DDSs have enjoyed considerable attention owing to their significant in drug delivery to target cells [10]. However, low drug loading efficiency, high toxicity, and immunogenicity are some of the major drawbacks to many of these systems [11, 12]. Researchers have investigated nanocarriers in order to correct the defects in anti-cancer drugs such as lack of selectivity, severe toxicity, low water solubility, and severe side effects [13-16].

Nowadays, nanotechnology is helping to significantly advance and revolutionize numerous technology and industry sectors, including information technology, food safety, environmental science [17-22], transportation, medicine, and energy [23-26]. Many research groups and scientists have found that one-dimensional (1D) nanostructures are encouraging DDSs for many drugs [27]. The most widely employed 1D nanostructures as DDSs are carbon nanotubes (CNTs) [28]. Nonetheless, many chemicals have a weak interaction with pure CNTs. This makes it almost impossible to employ CNTs as ideal DDSs [29, 30]. So, methods such as doping of impurities, chemical functionalization and generation of structural defects were adopted to resolve the above-mentioned problem [31-34]. Furthermore, impurity atoms such as Zn or O have been substituted for C atoms in diverse C-like nanotubes [35, 36]. One of the most commonly used nano-structures is ZnO nanotube (ZnO-NT), which has been successfully synthesized [37]. The ZnO-NT has a

large bandgap and polar Zn-O bonds, demonstrating its potential application in semiconductor-based DDSs. There are numerous studies on the interaction between ZnO-NT and different chemical agents. A pure ZnO-NT (PZnO-NT) cannot be considered as a suitable DDS in most cases because its stability is high and its tendency to have a reaction with different chemicals is less. Nonetheless, manipulating the structure of nanomaterials have been shown to be effective in boosting their reactivity to different chemicals [38, 39]. Here, density functional theory (DFT) computations are undertaken to investigate the interaction between PB and PZnO-NT, and X-doped (X = Al, Ge, and In) ZnO-NTs (X@ZnO-NTs) to find a DDS.

2. Computational details

In order to precisely describe the molecular properties of nanostructures, one of the commonly used density functionals is B3LYP. Nevertheless, estimation of dispersion interactions is one of its main drawbacks. Hence, we assessed the dispersion forces by including the Grimme's "D" [40]. The basis set (BS) utilized in this study is 6-31++G** (d) and the software used to undertake the computations is GAMESS [41]. The LANL2DZ BS is applied for the transition metals [42]. Moreover, the GaussSum program is used for the drawing of density-of-states (DOS) diagrams [43]. Based on the previous studies, B3LYP is one of the common functionals used to describe nanostructures due to its high accuracy [44, 45]. We computed the adsorption or adhesion energy (AdE) related to a PB drug on the nanotube surface through Eq. 1:

$$AdE = E(PB/ZnO\text{-}NT) - E(PB) - E(ZnO\text{-}NT) + E_{BSSE} \quad (1)$$

where E(PB/ZnO-NT) represents the energy of the ZnO-NT onto which a PB molecule was adhered. E(PB) is the energy of PB. E(ZnO-NT) is the energy of the pure ZnO-NT. E_{BSSE} has been computed by adopting the counterpoise method for all interactions [46]. The harmonics have been

estimated to verify that all geometries have positive frequencies. Eq. 2 was used to estimate the bandgap between the HOMO and the LUMO:

$$E_g = E_{LUMO} - E_{HOMO} \quad (2)$$

where E_{LUMO} and E_{HOMO}, respectively, are the energies of the lowest unoccupied and the highest occupied molecular orbitals.

3. Results and discussions

3.1. The characteristics of the nanotube and PB

The PB adhesion onto the nanotube surface (Fig. 1) was examined by choosing a ZnO-NT model (36 Zn and 36 O atoms). ZnO-NTs have been previously employed to adsorb various chemicals such as NO, N_2O_2, CO_2, CO, H_2O_2, N_2O, and NH_3 [47-50]. Moreover, the predicted diameter of ZnO-NT and the Zn-O bond length have been 8.81, and 1.92 Å, respectively, which were similar to those in experimental studies, i.e., 1.92 Å for Zn-O bond length [47]. According to the DOS diagram in Fig. 1, the LUMO energy is -2.54 and the energy of the HOMO is -6.36 eV for ZnO-NT (Table 1). So, the energy gap is around 3.82 eV. According to Fig. 2, there are several functional groups on the hexagonal ring of PB. We observed an HOMO profile within the PB structure, a site which was suitable for attacking the Zn atoms of ZnO-NT (Fig. 2).

3.2. The interaction between PZnO-NT and PB

The initial stage in DDSs is the adhesion of a drug to a carrier. We explored the PB adhesion on the PZnO-NT. The adhesion of PB on PZnO-NT is examined by placing a PB molecule at different sites (i.e., over Zn or O atoms, over a hexagon center and over the bridge of bonds). The PB was positioned on the PZnO-NT perpendicularly or in a parallel manner. According to Fig. 3, after the

initial geometry optimization, three local minima are predicted. The adhesion energy values of all complexes (CMPLs, Table 1) revealed that the PB adhesion to the ZnO-NT is weak and AdE ranges from -5.2 to -6.9 kcal/mol.

According to Fig. 3, in CMPL **T** (the CMPL with most stability), PB has a perpendicular interaction with the ZnO-NT surface and the distance is 3.76 Å for one O atom, and adhesion energy is -6.9 kcal/mol. As shown, PB somehow shared the O lone pairs with the Zn atoms. The NBO charge transfer from PB to the nanotube was 0.09 |e|, indicating the physical adhesion of PB to the ZnO-NT. There was a decrease in the bandgap from 2.82 eV in the PZnO-NT to 3.50 eV in CMPL **T**. The data for other CMPLs are provided in Table 1 and Fig. 3. The more stability of the CMPL **T** than another CMPLs can be ascribed to the HOMO of PB which was chiefly located on the O atom. As provided in Table 1, not any appreciable change occurred in the electronic attributes of ZnO-NT following the adhesion of PB. In addition to this, the less negative adhesion energy values, the very low adhesion capacity of ZnO-NT and the weakness of the interaction. Hence, the possibility of using the pure ZnO-NT as a proper nanocarrier for PB is low. The ZnO-NT was doped with the X atom to resolve the problem and boost the adhesion capacity and the interaction strength.

3.4. X-doping in the ZnO-NT structure

In order to boost the low reactivity of ZnO-NT towards PB, an X atom was substituted for O (NT **E**) and Zn atoms (NT **F**) in the ZnO-NT. Then, its impact was inspected on the electronic attributes and the geometric structure (GS) of the ZnO-NT (Fig. 4). The X atom caused a disruption in the ZnO-NT structure because the size of X atom is larger than the size of Zn and O atoms. This caused the X atom to project out of the surface of the ZnO-NT.

We inspect the stability of X-doped ZnO-NT (X@ZnO-NT) by computing the standard enthalpy of formation ($\Delta_f H^0$). Subtracting the deliberate atomization energy (ΣD_0) from the separated atoms' known enthalpy of formation yielded the theoretical enthalpy of formation at 298 K. For any X@ZnO-NT, $\Delta_f H^0$ at 298 K for one atom was given by [51]:

$$\Delta_f H^0 (X@ZnO\text{-}NT) = \Delta_f H^0 (X) + r\, \Delta_f H^0 (Zn) + t\, \Delta_f H^0 (O) - \Sigma D_0 \quad (3)$$

Here, r is the number of Zn atoms and t is the number of O. The estimated $\Delta_f H^0$ for Al, Ge, and In replaced instead of O atom in ZnO-NT, respectively, was -79.5, -82.4, and -97.1 kcal/mol. $\Delta_f H^0$ for Al, Ge, and In replaced instead of Zn atom in ZnO-NT, respectively, was -84.2, -91.3, -100.3 kcal/mol. In conclusion, NT **F** was thermodynamically more stable than NT **E**. Equation 4 was used to compute the standard Gibbs free energy of formation ($\Delta_f G^0$) for these two NTs in order to understand the entropic effect on their stability:

$$\Delta_f G^0 (In@ZnO\text{-}NT, 298\ K) = \Delta_f H^0 (In@ZnO\text{-}NT, 298\ K) - 298\ \Delta S \quad (4)$$

Here, ΔS is the change in entropy. The estimated $\Delta_f G^0$ for NTs **E** and **F** (In@ZnO-NT), respectively, was -18.9 and -50.3 kcal/mol, respectively. Here, the negative values demonstrate that the formation of In@ZnO-NT from the atoms is favorable thermodynamically, particularly in the NT **F**, in which a Zn atom was replaced by an X atom. The electron transfer from O atoms to the metal atoms could be the possible reason for the greater stability of NT **F** than NT **E**. Thus, NT **F** was selected to see how PB was adsorbed. The length of Al-O, Ge-O, and In-O bonds are about 2.95, 3.08, and 3.34 Å, respectively, in NT **F**. These bonds were are longer compared to Zn-O bonds. Doping the X atom appreciably reduced the bandgap of ZnO-NT (see Table 2) thanks to the appreciable change in the HOMO to lower energies following X-doping. After its doping, the X@ZnO-NT changed into a p-type semiconductor.

Different orientations were taken into account to place a PB above the X atom to inspect the interaction between PB and the X@ZnO-NT (NT **F**). Following the optimization of structures, one of the orientations was a local minimum, namely; PB/X@ZnO-NT (Fig.5). In this CML, the PB was placed at the top of the X atom with the bond length of 3.11, 3.03, and 2.92 Å for PB/Al, Ge, In@ZnO-NT, respectively. According to the NBO analysis, the partial positive charge of Al, Ge, and In was 0.64, 0.67, and 0.73 |e|, respectively. As a result, the PB could be adhered onto the X atom from the O atom PB (HOMO head) (Fig. 2). For PB/Al, Ge, In@ZnO-NT, the AdE is -26.4, -28.7, and -31.5 kcal/mol, respectively. Based on the results, doping the X atom led to an appreciable increase in the reactivity of the ZnO-NT toward the PB in comparison with the PZnO-NT. Electronic property analysis was carried out to verify this.

According to Table 2, a change was observed in the electronic attributes of the X@ZnO-NT following the adhesion of PB. The NBO charge transfer of about 0.26, 0.31, and 0.37 |e| occurred from the drug to the Al, Ge, and In, respectively. There was substantial destabilization in the HOMO level of X@ZnO-NT in the range of 27 to 34% following the adhesion of PB (see Table 2, and Fig. 6 for In@ZnO-NT). This substantial destabilization could be due to the nucleophilic nature of PB attacking the HOMO of the X@ZnO-NT (Fig. 7), which led to a substantial change in its energy. Nonetheless, modifying the electronic attributes of a material is one of the effective ways for DDSs and electronically harmless adhesion processed are considered ideal.

3.5. The influence of solvent on the adhesion

The solute-solvent interactions are responsible for the significant changes in the chemical and physical characteristics of the solute in going from gas phase to solvent phase [52-54]. Here, the influence of the H_2O solvent (HS) on the adhesion of PB to the In@ZnO-NT (for instance) was

inspected through the PCM [55]. For this purpose, the structures of PB, In@ZnO-NT, and CMP of PB/In@ZnO-NT were reoptimized in the HS. The findings revealed that the adhesion got weak and a change was observed in adhesion energy from -31.5 to -29.8 kcal/mol. Thus, it could be expressed as Eq. 3:

$$\Delta E_{sol\text{-}gas} = AdE\,(HS) - AdE\,(gaseous\ phase) = 1.7\ kcal/mol \quad (3)$$

here $\Delta E_{sol\text{-}gas}$ denotes the differences between the adhesion energy of PB in the gaseous phase (G-P) and in the HS. ΔE_{sol} (energy of solvation) of PB, In@ZnO-NT, and PB/In@ZnO-NT CMPs was calculated using Eq. 4:

$$\Delta E_{sol} = E_{sol} - E_{gas} \quad (4)$$

Here, the energies of a species in the G-P and in the HS and are represented by E_{gas} and E_{sol}, respectively. The ΔE_{sol} of In@ZnO-NT, PB, and PB/In@ZnO-NT, respectively, are -11.1, -6.1, and -12.2 kcal/mol, which demonstrate that the sum of E_{sol} of In@ZnO-NT and PB was more negative than the E_{sol} of PB/In@ZnO-NT. Indeed, In@ZnO-NT and PB were highly polar with an electric dipole moment, which made them more soluble in the polar HS. Hence, H_2O molecules surrounded PB and In@ZnO-NT forcefully, thus, preventing their interactions. Unlike in the GP, there was a slight change in the bandgap of In@ZnO-NT following its interaction with PB in the HS (around -0.09 eV). So, a negligible decrease was observed in the sensing response of In@ZnO-NT to PB in the HS.

3.6. The release of PB

The X@ZnO-NT is ideal for the adhesion of PB, which is the most pivotal step in DDSs. However, one of the challenges in DDSs is the release of drug from a carrier in target cells. The pH of normal cells is in fact more than the pH of tumor cells, showing that the environment of tissues has a pH

below 6 [56]. The influence of pH on the CMP (with most stability) between the In@ZnO-NT (for example) and PB was examined. We assume that H^+ species tend to attach to the nucleophilic heads of PB. So, we protonated the O atom of PB and performed the optimization computations. As a result, the AdE changes in the acid milieu from -31.5 to -20.2 kcal/mol and the distance between PB and the In@ZnO-NT increases to 3.54 Å. Also, according to Fig. 8, the interaction nature changes from a covalent bond (CB) to the H-bond (HB), which separates PB from the carrier via protonation. The protonated PB could not attach to the carrier, and it had to be released.

4. Conclusions

The potential use of PZnO-NT and X@ZnO-NT as drug carriers was investigated by examining the adhesion of PB to their surface. The interaction of PZnO-NT with PB was weak. However, after doping the X atom, the O atom of PB interacted with the X atom of the Al, In and Ge with AdE of about -26.4, and -31.5 and -28.7 kcal/mol, respectively. The mechanism of interaction changed from CB in blood cells to HB in cancerous cells, which could separate PB from In@ZnO-NT in cancerous cells with a low pH via protonation. The HB energy was very low, which was about -20.2 kcal/mol. The PCM was used to examine the solvent effect on the drug AdE on the In@ZnO-NT, indicating that it is about -29.8 kcal/mol. Overall, the results suggested the potential use of X@ZnO-NT (especially In@ZnO-NT) as an encouraging nanocarrier for PB delivery.

References

[1] E.R. Fox, L.S. Tyler, Managing drug shortages: seven years' experience at one health system, American journal of health-system pharmacy, 60 (2003) 245-253.

[2] X. He, T. T. Batchelor, S.Grossman, J. G. Supkoafor, Determination of procarbazine in human plasma by liquid chromatography with electrospray ionization mass spectrometry. J. Chromatogr. B., 799 (2004) 281-291.

[3] R. M. Gorsen, A. J. Weiss, R. W. Manthei, Analysis of Procarbazine and Metabolites by Gas Chromatography-Mass Spectrometry. J. Chromatogr., 221 (1980) 309-318.

[4] P. Rainer, B. Frank, R. Ralf, M. Michael, Plasma kinetics of procarbazine and azo-procarbazine in humans. Anti-Cancer Drugs., 17 (2006) 75-80.

[5] D. F. Lehmann, T. E. Hurteau, N. Newman, T. E. Coyle, Anticonvulsant usage is associated with an increased risk of procarbazine hypersensitivity reactions in patients with brain tumors. Clin. Pharmacol. Ther., 62 (1997) 225-229.

[6] S. Clifford Schold, T. P. Brent, E. Hofe, H. S. Friedman, S. Mitra, D. D. Bigner, J. A. Swenberg, D.V.M., P. Kleihues, M.D. 1O6-Alkylguanine-DNA alkyltransferase and sensitivity to procarbazine in human brain-tumor xenografts. Superlattices Microstruct., 70 (1989) 573-577.

[7] W.W.M. Formulary, Stuart, MC, Kouimtzi, M., Hill, SR, Eds, World Health Organization: Geneva, Switzerland, (2009).

[8] S. Moloney, R. Prough, Studies on the pathway of methane formation from procarbazine, a 2-methylbenzylhydrazine derivative, by rat liver microsomes, Archives of Biochemistry and Biophysics, 221 (1983) 577-584.

[9] B. Farhang Rik, R. Ranjineh Khojasteh, R. Ahmadi, M. Karegar Razi, Evaluation of C60 nano-structure performance as nano-carriers of procarbazine anti-cancer drug using density functional theory methods, Quarterly Journal of Iranian Chemical Communication, 7 (2019) 405-414.

[10] I. Hammadi Fahad, N. Sadoon, M.M. Kadhim, A. Abbas Alhussainy, S.K. Hachim, M. Abdulwahid Abdulhussain, S.A.H. Abdullaha, A. Mahdi Rheima, Potential of zinc carbide 2D monolayers as a new drug delivery system for nitrosourea (NU) anti-cancer drug, Computational and Theoretical Chemistry, 1217 (2022) 113927.

[11] M. Ibarra-Rodríguez, M. Sánchez, Adsorption of adrucil on [La-CTF-0]3+ system for drug delivery by density functional theory, Computational and Theoretical Chemistry, 1201 (2021) 113294.

[12] M. Adel, M.M. Kadhim, H.H. Muttashar, S.K. Hachim, S.A. Abdullaha, A.M. Rheima, Two-dimensional silicon carbide monolayer as a promising drug delivery vehicle for hydroxyurea anti-cancer drug, Korean Journal of Chemical Engineering, 40 (2023) 1433-1439.

[13] M. Perveen, L. Noreen, M. Waqas, R.F. Mehmood, J. Iqbal, S. Manzoor, S. Nazir, A.M. Shawky, R.A. Khera, A DFT approach for finding therapeutic potential of graphyne as a nanocarrier in the doxorubicin drug delivery to treat cancer, Journal of Molecular Graphics and Modelling, 124 (2023) 108537.

[14] A.T. Jalil, S.N. Thabit, Z.K. Hanan, M.Q. Alasheqi, A.K.J. Al-Azzawi, R.S. Zabibah, A.A. Fadhil, Modulating gut microbiota using nanotechnology to increase anticancer efficacy of the treatments, Macromolecular Research, 31 (2023) 739-752.

[15] R. Mirsa, S. Acharya, S.K. Sahoo, Cancer nanotechnology: application of nanotechnology in cancer therapy, Drug. Discov. Today 15 (2010) 842–850.

[16] A.A. Rajhi, W.K. Salih, S.M. Mekkey, H.A. Dhahi, A. Shather, A.A. Duhduh, S. Alamri, Z.S. Abbas, Development of a drug delivery system for thioguanine-based anticancer drugs for enhancing their effectiveness, Inorganic Chemistry Communications, 155 (2023) 111022.

[17] X. Yue, N.L. Ma, C. Sonne, R. Guan, S.S. Lam, Q. Van Le, X. Chen, Y. Yang, H. Gu, J. Rinklebe, Mitigation of indoor air pollution: A review of recent advances in adsorption materials and catalytic oxidation, Journal of hazardous materials, 405 (2021) 124138.

[18] S. Ge, N.L. Ma, S. Jiang, Y.S. Ok, S.S. Lam, C. Li, S.Q. Shi, X. Nie, Y. Qiu, D. Li, Processed bamboo as a novel formaldehyde-free high-performance furniture biocomposite, ACS applied materials & interfaces, 12 (2020) 30824-30832.

[19] S. Ge, S.Y. Foong, N.L. Ma, R.K. Liew, W.A.W. Mahari, C. Xia, P.N.Y. Yek, W. Peng, W.L. Nam, X.Y. Lim, Vacuum pyrolysis incorporating microwave heating and base mixture modification: an integrated approach to transform biowaste into eco-friendly bioenergy products, Renewable and Sustainable Energy Reviews, 127 (2020) 109871.

[20] S.Y. Foong, R.K. Liew, Y. Yang, Y.W. Cheng, P.N.Y. Yek, W.A.W. Mahari, X.Y. Lee, C.S. Han, D.-V.N. Vo, Q. Van Le, Valorization of biomass waste to engineered activated biochar by microwave pyrolysis: Progress, challenges, and future directions, Chemical Engineering Journal, 389 (2020) 124401.

[21] S.S. Lam, P.N.Y. Yek, Y.S. Ok, C.C. Chong, R.K. Liew, D.C. Tsang, Y.-K. Park, Z. Liu, C.S. Wong, W. Peng, Engineering pyrolysis biochar via single-step microwave steam activation for hazardous landfill leachate treatment, Journal of hazardous materials, 390 (2020) 121649.

[22] W. Fan, T. Liu, F. Wu, S. Wang, S. Ge, Y. Li, J. Liu, H. Ye, R. Lei, C. Wang, An Antisweat Interference and Highly Sensitive Temperature Sensor Based on Poly (3, 4-

ethylenedioxythiophene)–Poly (styrenesulfonate) Fiber Coated with Polyurethane/Graphene for Real-Time Monitoring of Body Temperature, ACS nano, 17 (2023) 21073-21082.

[23] Z.D. Alhattab, A.M. Aljeboree, M.A. Jawad, F.S. Sheri, A.K. Obaid Aldulaim, A.F. Alkaim, Highly adsorption of alginate/bentonite impregnated TiO2 beads for wastewater treatment: Optimization, kinetics, and regeneration studies, Caspian Journal of Environmental Sciences, 21 (2023) 657-664.

[24] A.M. Aljeboree, Z.D. Alhattab, U.S. Altimari, A.K.O. Aldulaim, A.K. Mahdi, A.F. Alkaim, Enhanced removal of amoxicillin and chlorophenol as a model of wastewater pollutants using hydrogel nanocomposite: Optimization, thermodynamic, and isotherm studies, Caspian Journal of Environmental Sciences, 21 (2023) 411-422.

[25] M.A. Obaid, K.H. Harbi, A.N. Abd, Study the effect of antibacterial on the chemically prepared copper oxide, Materials Today: Proceedings, 47 (2021) 6006-6010.

[26] A. Aljeboree, S. Essa, Z. Kadam, F. Dawood, D. Falah, A. AF, Environmentally friendly activated carbon derived from palm leaf for the removal of toxic reactive green dye, International Journal of Pharmaceutical Quality Assurance, 14 (2023) 12-15

[27] M.M. Kadhim, T.Z. Taban, S.A. Abdullaha, N. Alnasoud, S.K. Hachim, S. Alomar, Application of zinc oxide nano-tube as drug-delivery vehicles of anticancer drug, Journal of Molecular Modeling, 29 (2023) 47.

[28] M. Adeli, F. Hakimpoor, M. Ashiri, R. Kabiri, M. Bavadi, Anticancer drug delivery systems based on noncovalent interactions between carbon nanotubes and linear–dendritic copolymers, Soft Matter, 7 (2011) 4062-4070.

[29] Z. Al-Sawaff, S. Dalgic, F. Kandemirli, Theoretical study of the adsorption of BMSF-BENZ drug for osteoporosis disease treatment on Al-doped carbon nanotubes (Al-CNT) as a drug delivery vehicle, European Journal of Chemistry, 12 (2021) 314-322.

[30] A. Elhissi, W. Ahmed, I.U. Hassan, V. Dhanak, A. D'Emanuele, Carbon nanotubes in cancer therapy and drug delivery, Journal of drug delivery, 2012 (2012).

[31] H. Kurban, S. Alaei, M. Kurban, Effect of Mg content on electronic structure, optical and structural properties of amorphous ZnO nanoparticles: A DFTB study, Journal of Non-Crystalline Solids, 560 (2021) 120726.

[32] İ. Muz, M. Kurban, The electronic structure, transport and structural properties of nitrogen-decorated graphdiyne nanomaterials, Journal of Alloys and Compounds, 842 (2020) 155983.

[33] İ. Muz, M. Kurban, A first-principles evaluation on the interaction of 1, 3, 4-oxadiazole with pristine and B-, Al-, Ga-doped C60 fullerenes, Journal of Molecular Liquids, 335 (2021) 116181

[34] A.A. Peyghan, H. Soleymanabadi, Adsorption of H2S at Stone–Wales defects of graphene-like BC3: a computational study, Molecular Physics, 112 (2014) 2737-2745.

[35] S. Dou, J. Xu, C. Yang, W.-D. Liu, I. Manke, W. Zhou, X. Peng, C. Sun, K. Zhao, Z. Yan, Dual-function engineering to construct ultra-stable anodes for potassium-ion hybrid capacitors: N, O-doped porous carbon spheres, Nano Energy, 93 (2022) 106903.

[36] V. Cretu, V. Postica, A. Mishra, M. Hoppe, I. Tiginyanu, Y. Mishra, L. Chow, N.H. De Leeuw, R. Adelung, O. Lupan, Synthesis, characterization and DFT studies of zinc-doped copper oxide nanocrystals for gas sensing applications, Journal of Materials Chemistry A, 4 (2016) 6527-6539.

[37] Y. Xing, Z. Xi, Z. Xue, X. Zhang, J. Song, R. Wang, J. Xu, Y. Song, S.-L. Zhang, D. Yu, Optical properties of the ZnO nanotubes synthesized via vapor phase growth, Applied Physics Letters, 83 (2003) 1689-1691.

[38] Y. Yang, Y. Zhao, M. Xing, C. Tian, F. Ahmadi Peyghan, Effects of Ag-decoration on the adsorption and detection of toxic OF2 gas on a GaN nanotube, Molecular Simulation, (2022) 1-9. https://doi.org/10.1080/08927022.2022.2095375

[39] A.A. Peyghan, H. Soleymanabadi, M. Moradi, Structural and electronic properties of pyrrolidine-functionalized [60] fullerenes, Journal of Physics and Chemistry of Solids, 74 (2013) 1594-1598.

[40] S. Grimme, Accurate description of van der Waals complexes by density functional theory including empirical corrections, Journal of computational chemistry, 25 (2004) 1463-1473.

GAMESS

[41] M.W. Schmidt, K.K. Baldridge, J.A. Boatz, S.T. Elbert, M.S. Gordon, J.H. Jensen, S. Koseki, N. Matsunaga, K.A. Nguyen, S. Su, T.L. Windus, M. Dupuis, J.A. Montgomery, J. Comp. Chem. 14 (1993) 1347–1363.

[42] C.E. Check, T.O. Faust, J.M. Bailey, B.J. Wright, T.M. Gilbert, L.S. Sunderlin, Addition of polarization and diffuse functions to the LANL2DZ basis set for p-block elements, The Journal of Physical Chemistry A, 105 (2001) 8111-8116.

[43] N. O'Boyle, A. Tenderholt, K. Langner, Cclib: a library for package-independent computational chemistry algorithms, J. Comput. Chem. 29 (2008) 839–845.

[44] A.A. Peyghan, M.T. Baei, S. Hashemian, ZnO nanocluster as a potential catalyst for dissociation of H2S molecule, Journal of Cluster Science, 24 (2013) 341-347.

[45] M. Noei, A.A. Peyghan, A DFT study on the sensing behavior of a BC2N nanotube toward formaldehyde, Journal of Molecular Modeling, 19 (2013) 3843-3850.

[46] S.F. Boys, F. Bernardi, The calculation of small molecular interactions by the differences of separate total energies. Some procedures with reduced errors, Molecular Physics, 19 (1970) 553-566.

[47] A.A. Peyghan, M. Noei, Electronic Response of Nano-sized Cages of ZnO and MgO to Presence of Nitric Oxide, Chinese Journal of Chemical Physics, 26 (2013) 231-236.

[48] A.A. Ibrahim, P. Tiwari, M. Al-Assiri, A. Al-Salami, A. Umar, R. Kumar, S. Kim, Z. Ansari, S. Baskoutas, A highly-sensitive picric acid chemical sensor based on ZnO nanopeanuts, Materials, 10 (2017) 795.

[49] S.E.r. Diltemiz, K. Ecevit, High-performance formaldehyde adsorption on CuO/ZnO composite nanofiber coated QCM sensors, Journal of Alloys and Compounds, 783 (2019) 608-616.

[50] H. Ma, Y. Hou, H. Fang, A. Sarkar, Investigation of the interaction of amphetamine drug with Zn12O12 nanocage: a quantum chemical study, Journal of Computational Electronics, 20 (2021) 1065-1071.

[51] M. Chase Jr, J. Curnutt, J. Downey Jr, R. McDonald, A. Syverud, E. Valenzuela, JANAF thermochemical tables, 1982 supplement, Journal of Physical and Chemical Reference Data, 11 (1982) 695-940.

[52] M. Kurban, B. Gündüz, Physical and optical properties of DCJTB dye for OLED display applications: experimental and theoretical investigation, Journal of Molecular Structure, 1137 (2017) 403-411.

[53] M. Kurban, B. Gündüz, Study of structural, optical properties and electronic structure of PTCDI-C5 organic nanostructure, Chemical Physics Letters, 691 (2018) 14-21.

[54] M. Kurban, B. Gündüz, F. Göktaş, Experimental and theoretical studies of the structural, electronic and optical properties of BCzVB organic material, Optik, 182 (2019) 611-617.

[55] B. Mennucci, J. Tomasi, R. Cammi, J. Cheeseman, M. Frisch, F. Devlin, S. Gabriel, P. Stephens, Polarizable continuum model (PCM) calculations of solvent effects on optical rotations of chiral molecules, The Journal of Physical Chemistry A, 106 (2002) 6102-6113.

[56] I. Parolini, C. Federici, C. Raggi, L. Lugini, S. Palleschi, A. De Milito, C. Coscia, E. Iessi, M. Logozzi, A. Molinari, Microenvironmental pH is a key factor for exosome traffic in tumor cells, Journal of Biological Chemistry, 284 (2009) 34211-34222.

Figure captions

Figure 1. Optimized structure of the ZnO nanotube (ZnO-NT) and its density of states (DOS). Distance is in Å.

Figure 2. Optimized structure of procarbazine (PB) drug and its HOMO profile.

Figure 3. Optimized structures of PB/ZnO-NT complexes. Distances are in Å.

Figure 4. Optimized structures of different X atom-doped ZnO-NT (X@ZnO-NT).

Figure 5. Optimized structures of PB/Al, Ge, and In@ZnO-NT complexes. Distances are in Å.

Figure 6. Partial DOS of the most stable PB/In@ZnO-NT complex.

Figure 7. The HOMO profile of the most stable PB/In@ZnO-NT complex.

Figure 8. The optimized structure of protonated PB and In@ZnO-NT, showing separation from each other in the acidic environment. Distance is in Å.

Table 1. The calculated adsorption energy (AdE) in kcal/mol, HOMO, LUMO energies, and HOMO-LUMO energy gap (E_g) of bare ZnO nanotube (ZnO-NT) and the procarbazine (PB) and ZnO-NT complexes in eV. Q is the charge on the molecules.

Structure	AdE	E_{HOMO}	E_{LUMO}	E_g	ΔE_g(%)	Q(e)
ZnO-NT	-	-6.36	-2.54	3.82	-	-
R	-5.2	-6.14	-2.54	3.60	-5.8	0.06
S	-6.1	-6.09	-2.53	3.56	-6.8	0.07
T	-6.9	-6.02	-2.52	3.50	-8.4	0.09

Table 2. The calculated adsorption energy (AdE) kcal/mol, HOMO, LUMO energies, and HOMO-LUMO energy gap (E_g) of X-doped ZnO-NT (X = Al, Ge, and In and X@ZnO-NT) and the PB complexes in eV. Q is the charge on the molecules.

Structure	AdE	E_{HOMO}	E_{LUMO}	E_g	ΔE_g(%)	Q(e)
Al@ZnO-NT	-	-5.15	-2.51	2.64	-	-
PB/Al@ZnO-NT	-26.4	-4.41	-2.49	1.92	-27.3	0.26
Ge@ZnO-NT	-	-5.12	-2.52	2.60		-
PB/Ge@ZnO-NT	-28.7	-4.28	-2.49	1.79	-31.2	0.31
In@ZnO-NT	-	-5.08	-2.48	2.60		-
PB/In@ZnO-NT	-31.5	-4.16	-2.45	1.71	-34.2	0.37

Figure 1.

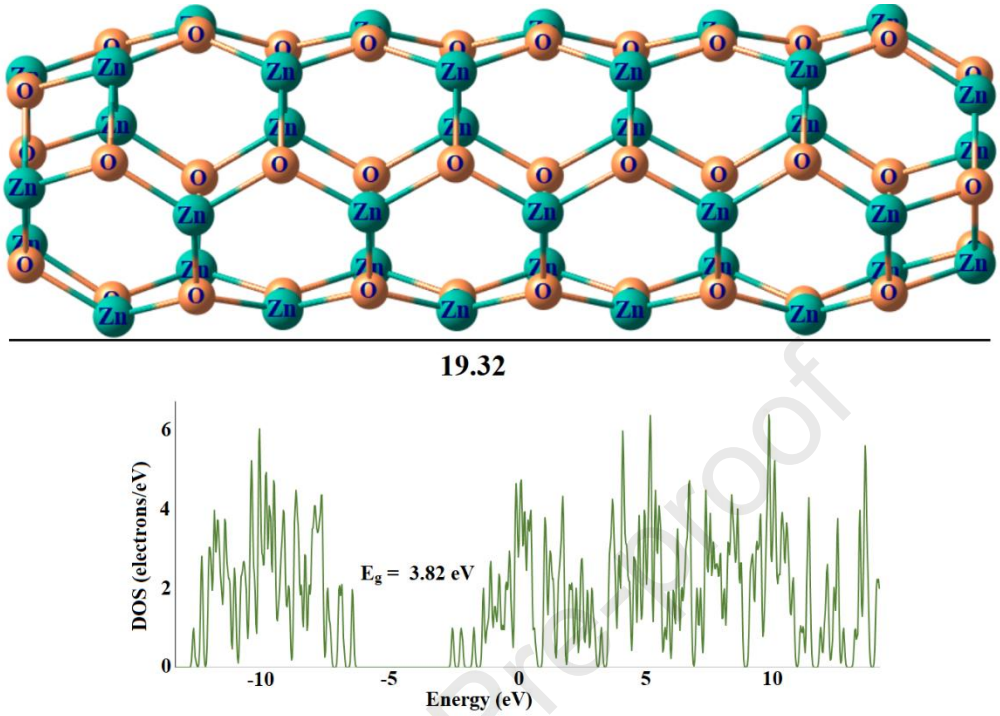

Figure 2.

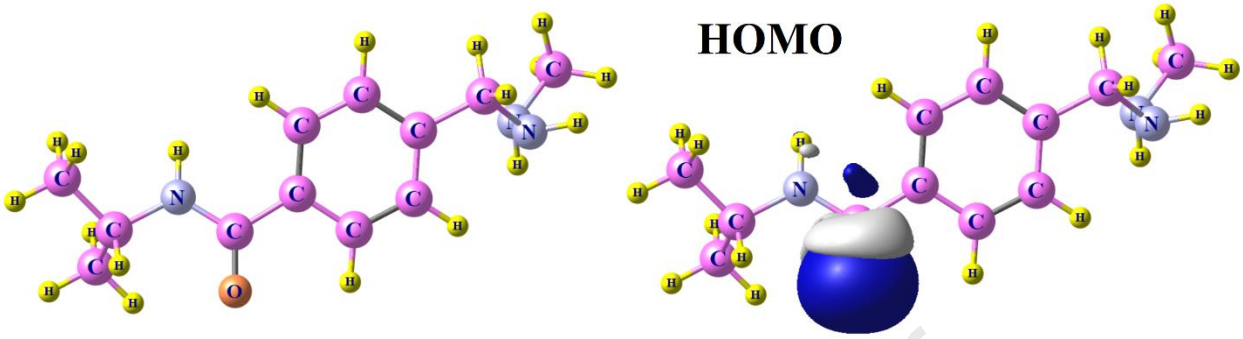

Figure 3.

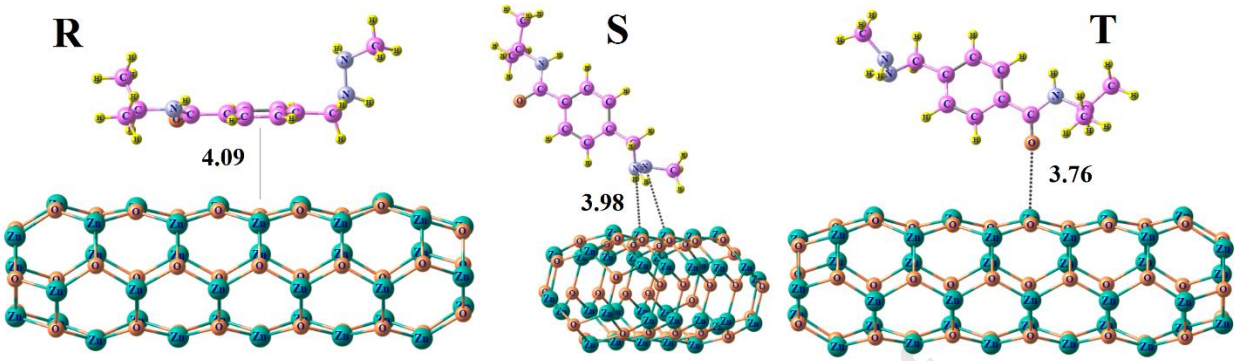

Figure 4.

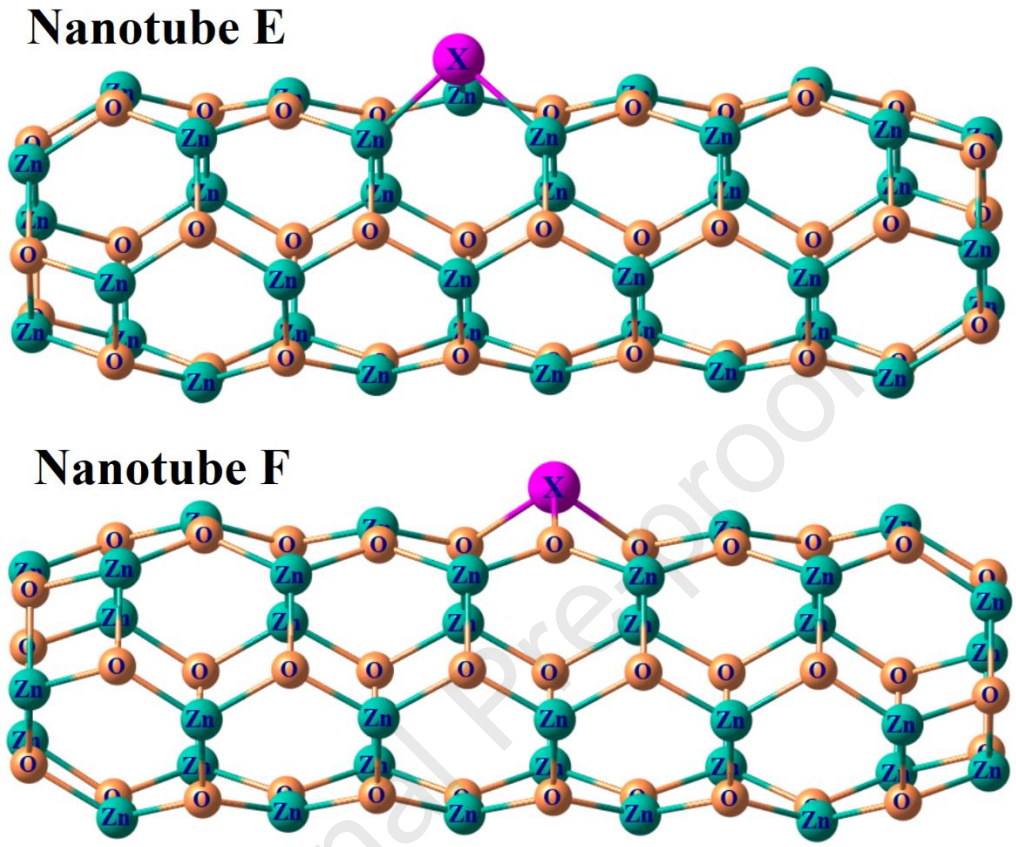

Figure 5.

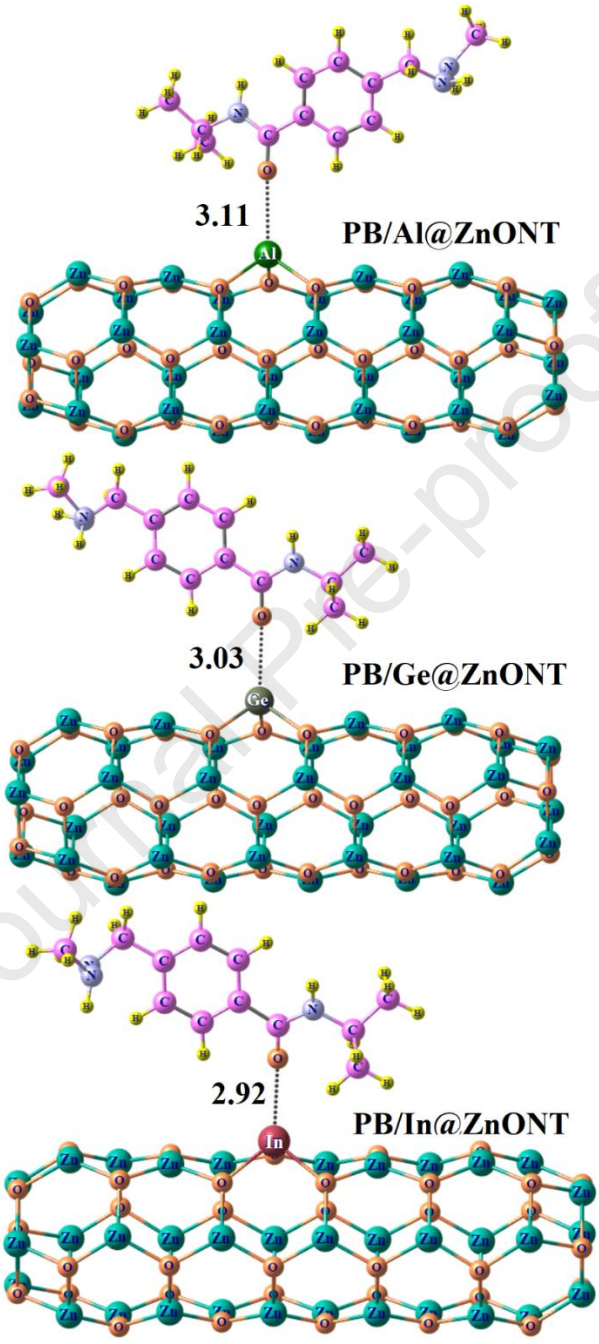

Figure 6.

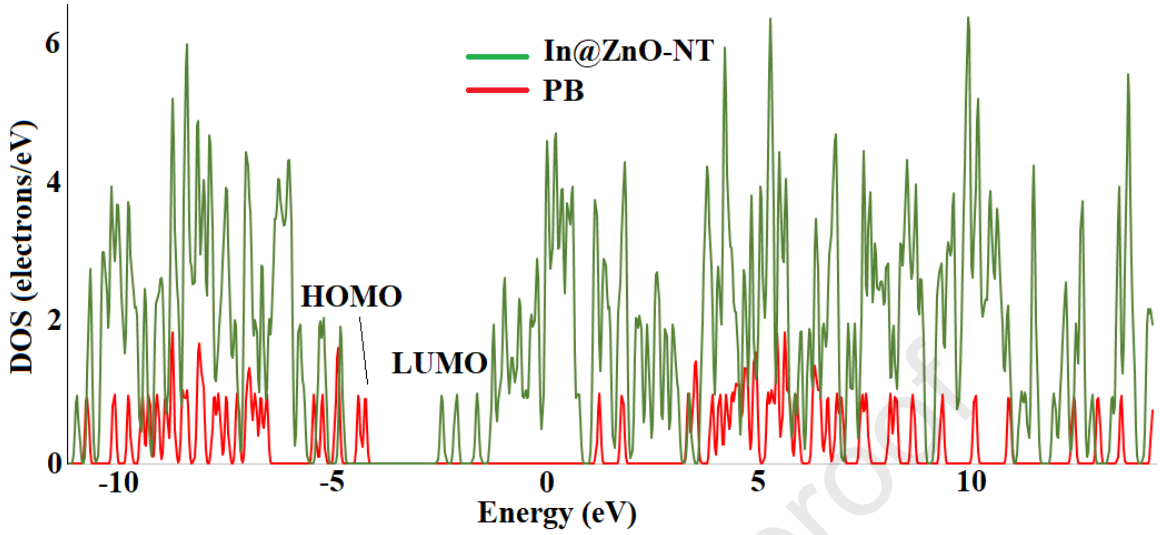

Figure 7.

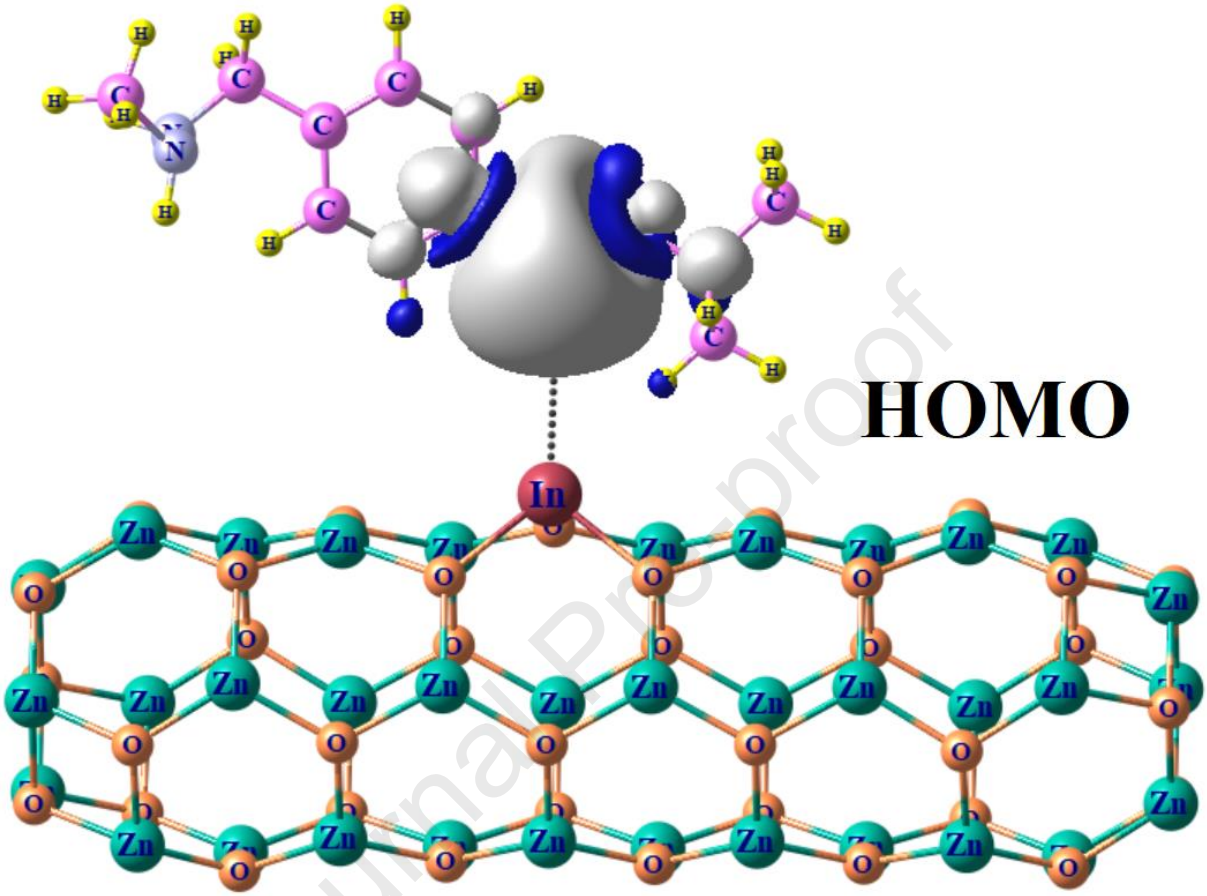

Figure 8.

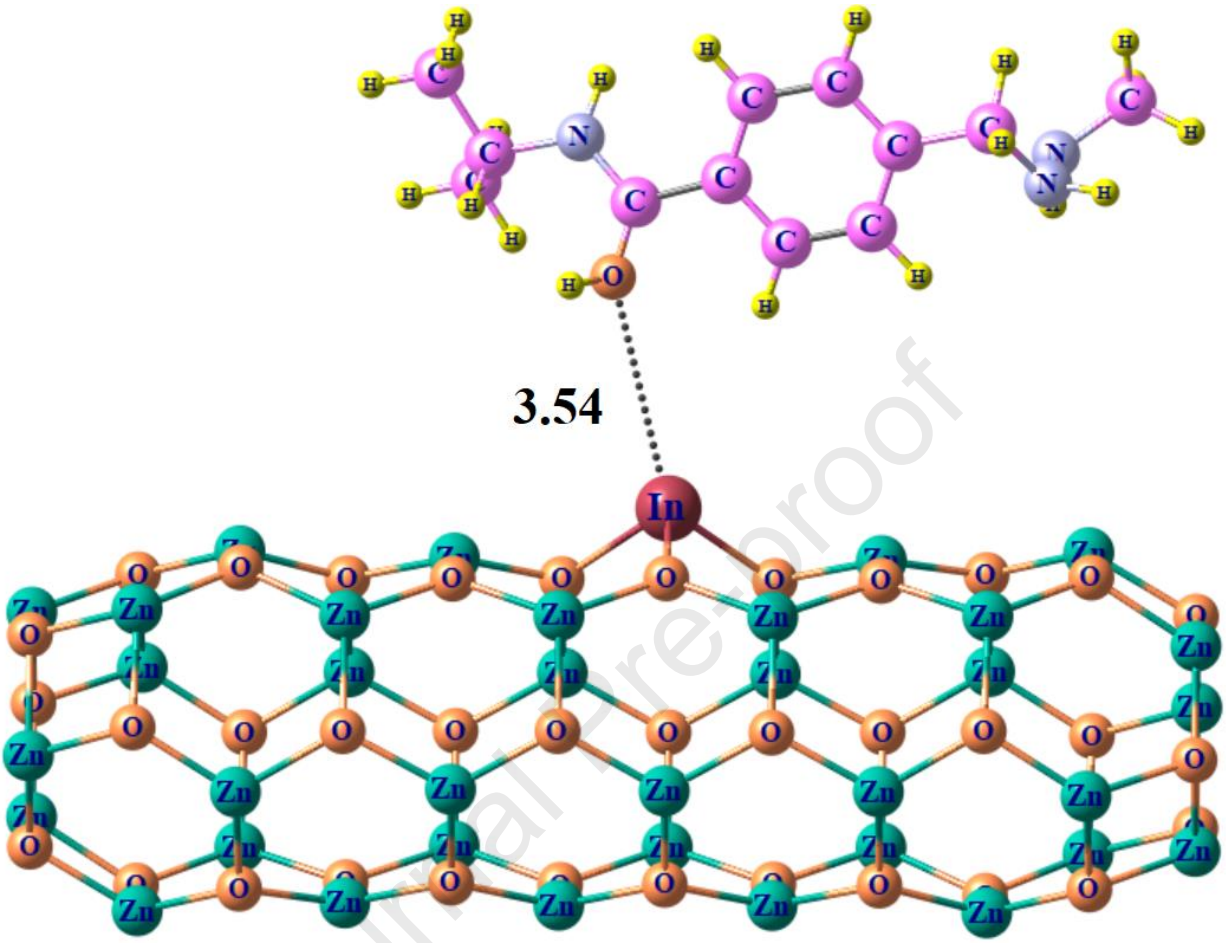

Declaration of interests

☒ The authors declare that they have no known competing financial interests or personal relationships that could have appeared to influence the work reported in this paper.

☐The authors declare the following financial interests/personal relationships which may be considered as potential competing interests: